Heterostructured high-T_c superconducting nanohybrid: $(Me_3S)_2HgI_4$-$Bi_2Sr_2CaCu_2O_y$

Soon-Jae Kwon*
Natural Science Research Institute, Jeonju University, Jeonju, Jeonbuk, 560-759, Korea

Jin-Ho Choy
National Nanohybrid Materials Laboratory, School of Chemistry and Molecular Engineering, Seoul National University, Seoul 151-747, Korea

Dongwoon Jung
Department of Chemistry, Wonkwang University, Iksan, Jeonbuk 570-749, Korea

Pham V. Huong
Laboratoire de Spectroscopie Moleculairé et Cristalline, Université Bordeaux I, 351, Cours de la Libération, 33405 Talence, France
(Received 22 April 2002; revised manuscript received 13 September 2002; published 27 December 2002)

We have developed a type of nanohybrid high-T superconductor with periodic stacking of the organic-salt layer and the superconducting cuprate one. Such a hybrid is realized by intercalative complexation, which means that complex formation proceeds in the interlayer space of two-dimensional solid lattice by reacting trimethylsulfonium iodide with the HgI_2-intercalated bismuth cuprate. The present organic-salt intercalate provides a clue to understand the high-T_c superconductivity in the layered cuprate and, at the same time, the synthetic strategy gives an interesting route to a different class of high-T_c superconducting nanohybrid. The powder x-ray-diffraction pattern shows that the organic-inorganic hybrid material features a stage-I intercalation compound with a basal increment of 12.6 Å compared to the pristine. The micro-Raman analysis reveals that the intercalated ionic sublattice consists of tetrahedral complex anion (HgI_4^{2-}) and organic cation (Me_3S^+), which is also cross confirmed by the extended x-ray-absorption fine-structure fitting results. In spite of large layer separation, the onset T_c of the nanohybrid is comparable to that of the pristine compound, unusual phenomena when compared with T_c depressions in the iodine-, AgI-, and HgX_2 (X=Br and I)-intercalated Bi-based cuprates.

DOI: 10.1103/PhysRevB.66.224510 PACS number(s): 74.72.Hs, 74.25.Jb, 74.25.Ha

I. INTRODUCTION

Intercalation technique applied to the layered high-T_c cuprate superconductors has been of crucial importance not only for the understanding of superconductivity in the layered cuprates but also for the practical application of high-T_c superconducting material.[1–11] In particular, the Bi-based cuprates $Bi_2Sr_2Ca_{m-1}Cu_mO_y$ ($m=1$, 2, and 3; BSCCO) have weakly bound Bi-O double layers, which leads to the expansion of the structure along the c axis leaving the internal structure of the cuprate lattice unchanged. While better understanding of high-T_c superconductivity in the layered cuprates was achieved both theoretically[12] and experimentally[13] through intercalation technique, no consensus has been reached as to the fundamental cause of this interesting phenomena. In order to further understand high-T_c superconductivity, it is of crucial importance to study materials with different degrees of coupling between the CuO_2 planes, i.e., with various interlayer distances. In this respect, free modulation of layer separation between cuprate blocks serves the twofold purpose of testing the mechanism responsible for superconductivity as well as developing multilayered nanohybrids with unprecedented structures. Recently we have synthesized two-dimensional (2D) superconductors by intercalating a long-chain organic compound into the Bi-based high-T_c cuprates *via* novel synthetic strategy of intercalative complexation.[4] The intercalation of organic moiety into the Bi-based cuprate allows us to easily control the interlayer distance and hence to provide an opportunity for probing the high-T_c mechanisms such as in-plane charge-carrier density[14,15] and interlayer electronic coupling between adjacent CuO_2 layers.[12,16] Consequently, the intercalation reaction becomes a powerful way of understanding the superconducting transition in the layered cuprate materials. Based on these motivations, we synthesized a different type of heterostructured nanohybrid $(Me_3S)_2HgI_4$-$Bi_2Sr_2CaCu_2O_y$ by the intercalation technique. The organic-salt could be intercalated into the $Bi_2Sr_2CaCu_2O_y$ (Bi2212) in the form of complex salt, bistrimethylsulfonium mercuric-tetraiodide $(Me_3S)_2HgI_4$. In this reaction scheme, the driving force of organic-salt intercalation is attributed to a large negative enthalpy change upon formation of complex anion in the interlayer space, $HgI_2+2I^-\rightarrow HgI_4^{2-}$, $\Delta H=-95.8$ kJ/mol.[17] The estimated mechanism of interlayer complexation is therefore as follows: first, when trimethylsulfonium iodide (Me_3SI) is reacted with HgI_2 intercalate (HgI_2-Bi2212), iodide anion (I^-) diffuses into the Bi-O double layers to make mercurictetraiodide anion of HgI_4^{2-} which is energetically more stable compared to the linear HgI_2 molecule. Then organic cation Me_3S^+ is followed to meet the charge neutrality condition in the intercalant layer.

The formation of single phase stage-I intercalation compound was confirmed by powder x-ray difraction (XRD) analysis. Micro-Raman and Hg L_{III}-edge x-ray-absorption

spectroscopic (XAS) analyses have been carried out not only to understand the formation mechanism of the intercalation complex but also to determine its intracrystalline structure. To investigate the superconducting properties, the magnetic susceptibilities for the pristine Bi2212 and its intercalates were measured using dc SQUID (superconducting quantum interference device) magnetometer. In addition, the x-ray-absorption near-edge structure (XANES) spectra for the I L_I-, Bi L_{III}-, and Cu *K*-edges were analyzed for the unintercalated and intercalated compounds in order to understand the effect of intercalation on the chemical interaction between host and guest, and consequently on the T_c evolution. We also combined theoretical calculations with experimental results to address the underlying questions regarding how the guest species interact with the host lattice.

II. EXPERIMENTAL DETAILS

A. Preparation and characterization of the samples

The polycrystalline Bi2212 compound was prepared by conventional solid-state reaction from the reagents of Bi_2O_3, $SrCO_3$, $CaCO_3$, and CuO with the nominal composition of Bi:Sr:Ca:Cu = 2:1.5:1.5:2, where Sr was partially substituted by Ca to obtain a single phase sample.[18] The starting reagents were thoroughly mixed and calcined at 800 °C for 12 h in air, and then the prefired material was pressed into disk-shaped pellets with 13 mm diameter, following the sintering process at 860 °C for 48 h with intermittent grindings.

The intercalation of organic moiety into the Bi-based cuprate was achieved with the following steps. At first, the HgI_2 intercalated Bi2212 $[(HgI_2)_{0.5}Bi_2Sr_{1.5}Ca_{1.5}Cu_2O_y$; HgI_2-Bi2212] was prepared by heating the polycrystalline Bi2212 and mercuric iodide in a vacuum-sealed Pyrex tube with the mole ratio of Bi2212:HgI_2=1:5 in the presence of 1 mole of free iodine $[P(I_2)\approx 1$ atm] as transporting agent. Two-step heat treatment was made at 190 °C for 2 h and at 240 °C for 4 h, and then the tube was placed in a temperature gradient in order to remove the excess mercuric iodide from the sample surface. Second, the $(Me_3S)_2HgI_4$ intercalate was synthesized by solvent-mediated reaction between preintercalated HgI_2-Bi2212 and Me_3SI, and the latter was formerly obtained by reacting iodomethane with 1 molar equivalent of dimethylsulfide in diethyl-ether solvent. The HgI_2-Bi2212 was mixed with three molar excess of Me_3SI, to which a small amount of acetonitrile (0.2 ml per 1 g of the mixture) was added. The mixture of reactants and solvent was heat treated in a sealed ampoule at 70 °C for 12 h. After the reaction had been completed, the sample was washed with acetonitrile to remove the excess reactant Me_3SI and dried in vacuum. From the electron probe microanalysis (EPMA) and elemental analyses for C, H, and S, the chemical formula of the present organic intercalate was determined to be $[(Me_3S)_2HgI_4]_{0.34}Bi_2Sr_{1.5}Ca_{1.5}Cu_2O_y$, denoted as $(Me_3S)_2HgI_4$-Bi2212. Here the chemical composition of the host is identical to nominal composition of the pristine within the limit of experimental error, indicating that the cuprate lattice has not chemically modified after the intercalation. The Raman spectra for the samples were recorded in the frequency range of 20–3600 cm^{-1}, using Laser Source Spectra Physics Model 2017 emitting at 514.532 nm with an intensity of 200 mW. The superconducting properties for the pristine and the intercalates were analyzed by measuring the dc magnetic susceptibilities in the temperature range 10–90 K with an applied magnetic field of 20 G.

B. X-ray-absorption measurement and data analysis

X-ray-absorption experiments were carried out with synchrotron radiation at the beam lines 7C and 10B in the Photon Factory (National Laboratory for High-Energy Physics, Tsukuba, Japan) operated at 2.5 GeV, 260~270 mA. Samples were finely ground, mixed with boron nitride (BN) in an appropriate ratio, and pressed into pellets, in order to obtain an optimum absorption jump ($\triangle\mu t\approx 1$) enough to be free from the thickness and pinhole effects.[19,20] All the XANES and x-ray-absorption fine-structure (EXAFS) spectra have been recorded in transmission mode for the Bi L_{III}-, Cu *K*-, Hg L_{III}-, and I L_I-edges at room temperature. The silicon (311) channel-cut monochromator was used for the Cu *K*-, Hg L_{III}-, and Bi L_{III}-edges, while silicon (111) double crystal monochromator, detuned to 60% of the maximum intensity to minimize the higher harmonics, was utilized for the I L_I-edge. To ensure the spectral reliability, much care was made to evaluate the stability of energy scale by monitoring the spectra of Cu metal and Bi_2O_3 for each measurement, and thus the edge positions were reproducible to better than 0.05 eV.

For the data analysis of the present XAS spectra, the inherent background in the data was removed by fitting a polynomial to the pre-edge region and extrapolated through the entire spectrum, from which it was subtracted. The resulting spectra $\mu(E)$ were normalized to an edge jump of unity for comparing the XANES feature with one another. The absorption spectrum for the isolated atom $\mu_\circ(E)$ was approximated by summing the cubic spline. The EXAFS oscillation $\chi(E)$ was obtained as $\chi(E)=\{\mu(E)-\mu_\circ(E)\}/\mu_\circ(E)$. The resulting data were converted into *k* space defined as $k=8\pi[2m_e(E-E_\circ)/h^2]^{1/2}$, where *k* is the wave vector, m_e the electron mass, and $E_\circ$ the threshold energy. The oscillating $\chi(k)$ function was weighted by a factor of k^3 to compensate the attenuation of EXAFS signal at the high *k* range with increasing photon energy and then Fourier transformed with a Hanning apodization function. In order to determine the structural parameters such as bond distance and coordination number, a nonlinear least-square fitting procedure was performed for the inverse Fourier transformed $k^3\chi(k)$ of the first shell in the Fourier transform by using the EXAFS formula based on the plane-wave single-scattering description, which can be expressed by the equation[21]

$$\chi(k)=-S_\circ^2\sum_i \frac{N_i}{kR_i^2}F_i(k)\exp\{-2\sigma_i^2k^2\} \times\exp\{-2R_i/\lambda(k)\}\sin\{2kR_j+\phi_i(k)\}, \quad (1)$$

where F_i (*k*) is the back scattering amplitude from each of the N_i neighboring atoms at a R_i distance with a Debye-

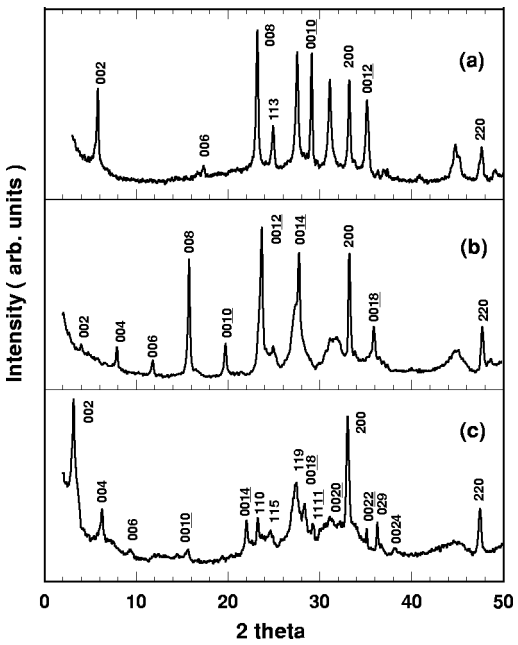

FIG. 1. Powder XRD patterns for (a) the pristine Bi2212, (b) HgI_2-Bi2212, and (c) $(Me_3S)_2HgI_4$-Bi2212.

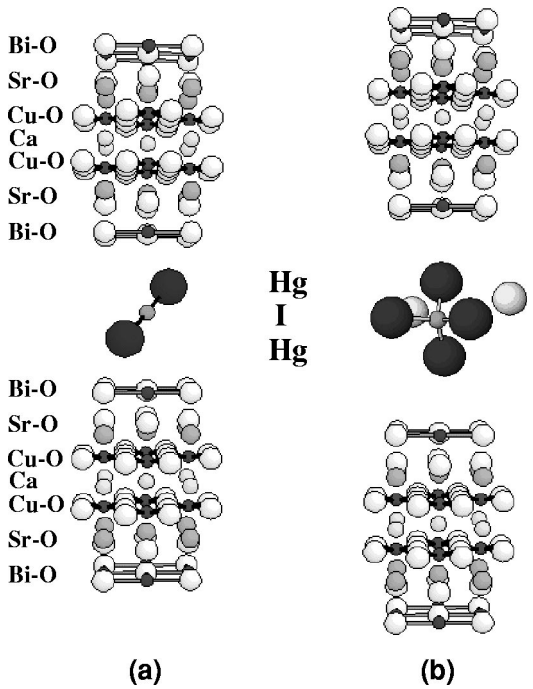

FIG. 2. The schematic structural models for (a) the HgI_2-Bi2212 and (b) the $(Me_3S)_2HgI_4$-Bi2212. The isolated circle in (b) represents the trimethyl sulfonium cation Me_3S^+.

Waller factor of σ_i^2, $S_\bigcirc$ is the amplitude reduction factor due to many-body effects, $\phi_i(k)$ is the total phase shift, and $\lambda(k)$ is the photoelectron mean free path. The curve fitting procedure was carried out by using $F_i(k)$, $\phi_i(k)$, and $\lambda(k)$, theoretically calculated by a curved wave *ab initio* EXAFS code FEFF 6.[22] The refinements were made by minimizing the F factor, defined by $F=(\Sigma\{k^3[\chi(k)_{cal}-\chi(k)_{exp}]\}^2/(n-1))^{1/2}$, where $\chi(k)_{cal}$, $\chi(k)_{exp}$, and n denote the experimental EXAFS oscillation, the fitted oscillation, and the number of data points, respectively.

In order to understand the different hole-doping effects upon HgI_2 and $(Me_3S)_2HgI_4$ intercalation, a theoretical estimation of electronic interaction between host and guest was performed for both types of intercalation compounds. Based on the ''extended Hückel tight-binding band'' calculation method, molecular orbitals (MO's) for the host and the guest were separately calculated, and the results were discussed in relation to the T_c evolution upon intercalation.

III. RESULTS AND DISCUSSION

A. X-ray-diffraction analysis

The formation of single phase stage-I intercalate was confirmed by XRD measurements using nickel filtered Cu-$K\alpha$ radiation with a graphite monochromator. The powder XRD patterns for the pristine Bi2212, HgI_2-Bi2212, and $(Me_3S)_2HgI_4$-Bi2212 are shown in Figs. 1(a)–(c), respectively. There is no trace of the pristine phase in the XRD patterns for all the present intercalates, indicating that mercuric iodide and organic salt are incorporated homogeneously into the host lattice. The broad background peak at around 30° in the 2θ range is attributed to the pulverization-induced fine particles during sampling for XRD measurement rather than the intrinsic amorphous components in the samples. According to the least-square fitting analysis of $(00l)$ reflection peaks, the intercalated organic-salt layer expands the unit cell along the c axis by 12.6 Å compared to the pristine, whereas the lattice is increased by 7.2 Å upon mercuric iodide intercalation. Although the intercalation of $(Me_3S)_2HgI_4$ remarkably increases the basal spacing of Bi2212, it has little effect on the in-plane lattice parameters. The a and b parameters of $(Me_3S)_2HgI_4$-Bi2212 determined from the (020) and (220) diffraction peaks are both 5.4 Å, invariant to those of the pristine compound. The existence of tetrahedral HgI_4^{2-} unit is confirmed not only by micro-Raman spectroscopy but also by Hg L_{III}-edge EXAFS analysis for $(Me_3S)_2HgI_4$-Bi2212. Based on these findings, the evolution of intracrystalline structure is schematically illustrated in Fig. 2, where the linear HgI_2 molecule is converted into the four-coordinated anion (HgI_4^{2-}) in-between the cuprate lattice.

B. dc magnetic susceptibility measurements

Zero-field-cooled (ZFC) dc magnetization of the pristine Bi2212, HgI_2-Bi2212, and $(Me_3S)_2HgI_4$-Bi2212 were measured as a function of temperature. As shown in Fig. 3, the present organic-salt intercalate exhibits the onset T_c of 81 K, which is higher than that of the HgI_2 intercalate (68 K), even slightly higher than the pristine Bi2212 (78 K). No obvious observation of two or more distinct transitions in the intercalation compounds indicates their homogeneity. The T_c variation in these intercalates can be explained as a result of modification of charge-carrier density in the CuO_2 layer, due to the charge transfer between cuprate lattice and guest. From previous studies on the wide class of high-T_c materials

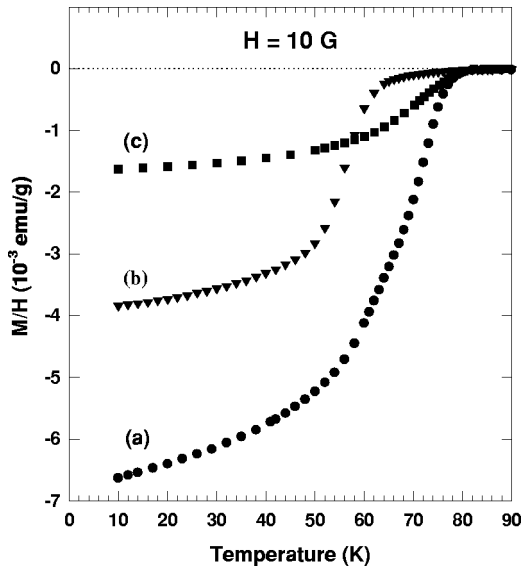

FIG. 3. Temperature-dependent ZFC magnetization M with an applied magnetic field of 10 G, measured with SQUID magnetometer. Data points represent (a) Bi2212 (●), (b) HgI_2-Bi2212 (▼), and (c) $(Me_3S)_2HgI_4$-Bi2212 (■).

including Bi2212, it is generally known that an universal parabolic curve for describing the relation between T_c and carrier density n is $T_c/T_{max}=1-82.6\,(n-0.16)^2$, where T_c goes up gradually and reaches a maximum (T_{max}), and then drops down as the carrier density increases.[14,23,24] Considering such a phenomenon, the T_c depression ($\Delta T_c \approx 10$ K) upon HgI_2 intercalation is surely attributed to an increased charge-carrier (hole) density in the CuO_2 layer, since the pristine compound prepared in air is in the region of hole overdoped state.[25] Based on the same ground, the T_c recovery upon Me_3SI intercalation can be also understood by the reduction of hole concentration in the CuO_2 plane. Here it is worthwhile to note that the T_c can be manipulated only by the intercalation reaction, in other words, the T_c value can be not only depressed but also raised depending on the chemical nature of the intercalant. It was previously found that upon iodine or mercuric iodide intercalation electrons are transferred from the host lattice to the guest.[6,13] In the present $(Me_3S)_2HgI_4$ intercalate, however, it is postulated that a partial electron transfer occurs from the guest to the host, which leads to a decrease in the hole density within CuO_2 plane and consequently to an increase in the T_c. Irrespective of T_c variation, diamagnetic-shielding magnitude decreases monotonously from the pristine Bi2212 through the HgI_2-Bi2212 and to the $(Me_3S)_2HgI_4$-Bi2212, as was clearly seen in Fig. 3. The shielding fractions were determined to be 42, 21, and 8% for the pristine Bi2212 ($d \approx 12$ Å), HgI2-Bi2212 ($d \approx 20$ Å), and (*Me*3S)2HgI4-Bi2212 ($d \approx 25$ Å), respectively, where d represents the distance between nearest CuO_2 planes belonging to the adjacent cuprate blocks. This result is attributed to an effect of layer separation between superconductively active CuO_2 layers, in the present case between CuO_2 bi-layers, on the tunneling supercurrent. Owing to the random orientation of microcrystals in these powder samples, the shielding effects are averaged over those of in-plane and out-of-plane (tunneling) supercurrents, where the latter is more drastically influenced by the layer separation than the former.[26–29] Therefore the systematic decrease of diamagnetic shielding magnitude with increasing interlayer distance is primarily related to a weakening of Josephson tunneling current due to the exponential dependence of tunneling probability on the barrier thickness,[26,30] although detailed studies will be required to elucidate this effect.

C. XAS analyses

Upon formation of $(Me_3S)_2HgI_4$ in-between Bi_2O_2 double layers, the pre-intercalated HgI_2 molecule reacts with two I^- anions to form a complex anion of HgI_4^{2-}. The information of local structure around Hg atom and its electronic configuration before and after the complex formation would be necessary not only to understand the reaction mechanism but also to correlate them with superconducting properties. However, the conventional spectroscopic method such as x-ray photoelectron spectroscopy (XPS) is not so effective to probe the bulk electronic structure of the intercalation compounds whose surface might be easily contaminated from the reactant. Moreover, it is difficult to determine the in-plane crystal structure by x-ray-diffraction method due to their high anisotropic nature. In this regard, x-ray-absorption spectroscopy is the most powerful way of examining not only an electronic structure of a specific atom by XANES but also a local geometry around absorber atom by EXAFS.[6,31–35]

In this work, the evolution of electronic and geometric structure of host and guest at each intercalation step has been examined by performing the systematic spectroscopic XANES/EXAFS analyses for I, Hg, Bi, and Cu. We have performed the curve fitting analysis to the Hg L_{III}-edge EXAFS spectra in order to determine the intracrystalline structure of the intercalated mercury species, which is very important to understand how they are stabilized inbetween the oxide block as well as to study physicochemical properties of the intercalates. The I L_I-edge XANES analysis has also been made to probe orbitals with p character which is the primary orbital relevant to the electronic interaction with the host lattice. Among various features in the L_I-edge spectra, the white line corresponding to the transition from $2s$ level to unoccupied np state above the Fermi level yields a direct measure on the degree of charge transfer between the cuprate lattice and the guest.

1. I L_I-edge XANES analysis

Figure 4 shows the I L_I-edge XANES spectra and their second derivatives for HgI_2-intercalate and the $(Me_3S)_2HgI_4$ one, together with I_2, HgI_2, $(Me_3S)_2HgI_4$, Me_3SI, and KI as reference compounds. All the spectra except for KI and Me_3SI exhibit a pre-edge peak A (so-called "white line"-type feature) in the 5185–5188-eV region, corresponding to the transition from the $2s$ core level to the $5p$ state above the Fermi energy level (E_F). As can be seen in Fig. 4, peak A shows a noticeable intensity for free I_2 with an unoccupied $5p$ state, whereas it disappears for ionic compounds such as

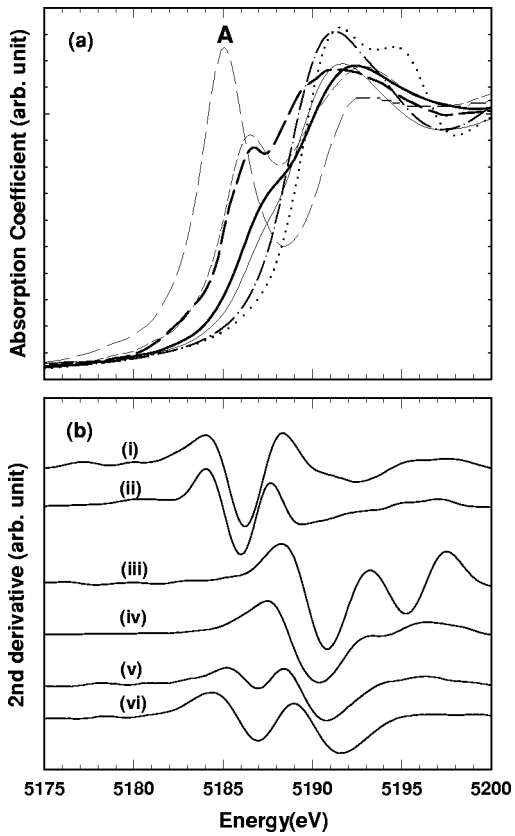

FIG. 4. (a) I L_I-edge XANES spectra for I_2 (lightface long-dashed line), HgI_2 (lightface short-dashed line), HgI_2-Bi2212 (boldface long-dashed line), KI (dotted line), Me_3SI (dash-dot line), $(Me_3S)_2HgI_4$ (lightface solid line), and $(Me_3S)_2HgI_4$-Bi2212 (boldface solid line). (b) Second derivative spectra for (i) HgI_2, (ii) HgI_2-Bi2212, (iii) KI, (iv) Me_3SI, (v) $(Me_3S)_2HgI_4$, and (vi) $(Me_3S)_2HgI_4$-Bi2212.

Me_3SI and KI with fully occupied $5p$ state. The HgI_2 and the $(Me_3S)_2HgI_4$ also represent distinct pre-edge peaks but with a slight depression in intensities, those which are attributed to the partially empty $5p$ state due to a strong covalent mixing between the Hg $6s$ orbital and the I $5p_z$ one.[36] These results are well understood as a combined effect of a highly polarizable I^- and Hg^{2+} ion with an electronic configuration of $[Xe]4f^{14}5d^{10}6s^0$, where d and f electrons shield the nucleus poorly, compared to the K^+ with a $[Ne]3s^23p^64s^0$ electronic configuration. Upon HgI_2 intercalation, the intensity of pre-edge peak A is rather suppressed when compared to that of free HgI_2, which is indicative of partial hole filling in the $5p$ state due to an electron transfer from the host lattice to the intercalated HgI_2 layer.[6] The change in oxidation state of iodine can be also probed from the variation of energy difference between the white line peak and the second absorption one at about 5190 eV corresponding to the transition to the unbound continuum state. As shown in Fig. 4(b), the continuum peak is shifted toward lower energy for the HgI_2 intercalate, whereas it is slightly shifted toward higher energy for the $(Me_3S)_2HgI_4$ intercalate, compared to those of free HgI_2 and $(Me_3S)_2HgI_4$ compounds. The transition energies of $2s\rightarrow 5p$ (E_{WL}) and $2s\rightarrow$ continuum state (E_C) are determined from the peak position in the first-derivative spectra for the HgI_2 series and in the second-derivative spectra for the $(Me_3S)_2HgI_4$ ones, as listed in Table I. It was previously known that the energy difference between the pre-edge and continuum peak ($\Delta E = E_{WL} - E_C$), which is associated with the energy gap between the highest occupied level and the unbound continuum state, is found to be inversely proportional to the electron density of antibonding state.[37] Therefore the decrease of energy difference (ΔE) in the HgI_2 intercalate compared to the free HgI_2, indicates the electron transfer from the cuprate block to the intercalated HgI_2 layer. In the $(Me_3S)_2HgI_4$ intercalate, however, the ΔE slightly increases with respect to the free $(Me_3S)_2HgI_4$, suggesting that electrons are transferred from the intercalated $(Me_3S)_2HgI_4$ layer to the host.

TABLE I. Edge energies of the I L_I-edge XANES spectral feature.

Compound	E_{WL} (eV)[a]	E_C (eV)[a]	ΔE (eV)
I_2	5185.0	5191.7	6.7
HgI_2	5186.2	5190.8	4.6
HgI_2-Bi2212	5185.8	5190.2	4.4
$(Me_3S)_2HgI_4$	5186.0	5189.3	3.8
$(Me_3S)_2HgI_4$-Bi2212	5186.1	5190.3	4.2

[a]Edge energies were determined from the peak positions in the first derivative spectra for I_2, HgI_2, and HgI_2-Bi2212 and in the second derivative one for $(Me_3S)_2HgI_4$ and $(Me_3S)_2HgI_4$-Bi2212, respectively.

As previously discussed,[6] a decrease in I L_I pre-edge peak intensity is related to the electronic charge transfer from the cuprate lattice to the intercalated HgI_2 layer, which explains the T_c depression ($\Delta T_c \approx 10$ K) in the HgI_2 intercalate. On the other hand, the intensity of pre-edge peak A in the $(Me_3S)_2HgI_4$-Bi2212 is more prominent than that in the free salt $(Me_3S)_2HgI_4$, suggestive of an electron transfer from HgI_4^{2-} to the host lattice. Therefore it is not so unreasonable to assume that the Bi-O and CuO_2 layers should be oxidized upon HgI_2 intercalation and reduced upon $(Me_3S)_2HgI_4$ intercalation. Actually, this postulation has been confirmed to be correct by the Bi L_{III}- and Cu K-edge XANES analyses for these intercalates, and also by molecular ortibal calculations based on the extended Hückel tight-binding band method.

2. Hg L_{III}-edge XANES and EXAFS

Figures 5(a) and (b) represent the Hg L_{III}-edge spline spectra and their second derivatives for the HgI_2 intercalate and the $(Me_3S)_2HgI_4$ one, respectively, together with the reference compounds, HgI_2 and $(Me_3S)_2HgI_4$. The Hg L_{III}-edge XANES spectrum offers qualitative information about the coordination geometry around the absorption atom. Since all the present compounds contain Hg^{+II} ion with vacant $6s$ and $6d$ orbitals, not only the main-edge peak corresponding to $2p_{3/2}\rightarrow 6d$ transition but also the pre-edge peak A corresponding to $2p_{3/2}\rightarrow 6s$ one is electric-dipole allowed ($\Delta l = l_f - l_i = \pm 1$).[21] According to the previous Hg L_{III}-edge

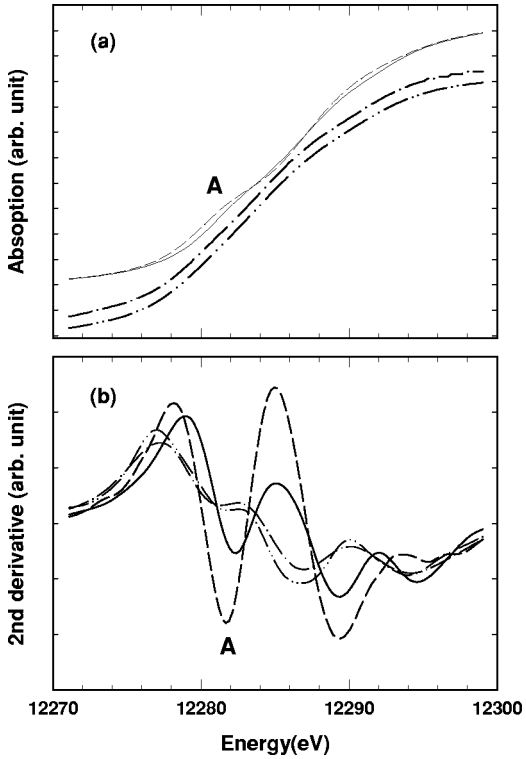

FIG. 5. (a) Hg L_{III}-edge XANES spectra and (b) their second derivatives for HgI_2 (solid line), HgI_2-Bi2212 (dashed-line), $(Me_3S)_2HgI_4$ (dash-dot line), and $(Me_3S)_2HgI_4$-Bi2212 (dash-dot-dot line).

XAS studies,[38,39] the intensity of pre-edge peak A at approximately 12 282–3 eV decreases with increasing coordination number around the mercury ion, i.e., linear > tetrahedral > octahedral, due to an increased Rydberg-like character of the excited orbitals for the higher coordination numbers. In this respect, an enhanced pre-edge peak in the HgI_2 intercalate compared with that in the free HgI_2 demonstrates a decrease of coordination number around mercury atom upon intercalation of HgI_2 into the cuprate lattice. Although the pre-edge peak A in the HgI_2-Bi2212 is quite enhanced, the peak intensity in the $(Me_3S)_2HgI_4$-Bi2212 is strongly depressed as can be clearly seen in Fig. 5(b), indicative of an increase of coordination. Even though previous crystallographic studies revealed that both the free HgI_2 solid and the $(Me_3S)_2HgI_4$ salt have HgI_4 tetrahedron,[40,41] the intensities of pre-edge peak A are nearly vanished not only for the $(Me_3S)_2HgI_4$ but also for the $(Me_3S)_2HgI_4$-Bi2212 when compared to HgI_2. This attenuation of $2p_{3/2} \rightarrow 6s$ transition is attributed to a decreased vacancy of Hg $6s$ orbital in the tetrahedral HgI_4^{2-} anion for both the organic salt and its intercalate, in which iodide anions (I^-) provide electron density more favorably to the Hg^{II+} valence shell through Hg $6s-I5p_z$ covalent bonding[42] than those in free HgI_2 solid.

Hg L_{III}-edge EXAFS analysis has been carried out to solve the intracrystalline structure of the guest species quantitatively. The Fourier transforms (FT's) of the k^3-weighted Hg L_{III}-edge EXAFS spectra for HgI_2- and $(Me_3S)_2HgI_4$ intercalates, together with that of free salt $(Me_3S)_2HgI_4$, are shown in Fig. 6(a). In the Fourier transforms of the present

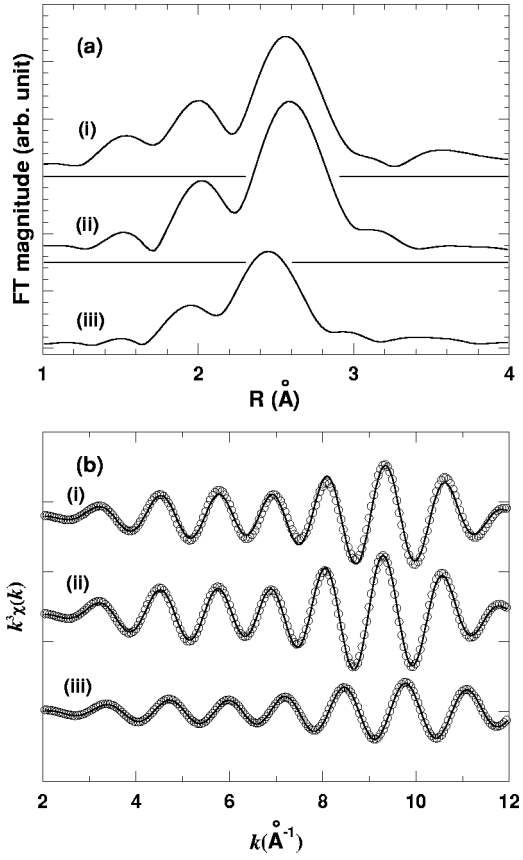

FIG. 6. (a) Fourier transformation of k^3-weighted Hg L_{III}-edge EXAFS in R space for (i) $(Me_3S)_2HgI_4$-Bi2212, (ii) free $(Me_3S)_2HgI_4$, and (iii) HgI_2-Bi2212. (b) Their Fourier filtered EXAFS oscillations, where the solid lines and empty circles represent the fitted and experimental data.

Hg-I species, a doubly split feature is observed at around 2.0 and 2.6–2.8 Å. Such a peak splitting is attributed to the Ramsauer-Townsend resonance which occurs generally in the backscattering amplitude of heavy atom with high atomic number.[43] The first coordination shell of the mercury-iodine (Hg-I) bond was isolated by inverse Fourier transformation to k space. The resulting $k^3\chi(k)$ Fourier filtered EXAFS oscillations are shown in Fig. 6(b), and the curve fittings for them were performed in order to determine the structural parameters such as coordination number (N), bond length [R(Hg-I)], and Debye-Waller factor (σ^2). The amplitude of EXAFS oscillation is increased for the $(Me_3S)_2HgI_4$ intercalate compared to the HgI_2 one, which indicates an increase of coordination number around Hg. In general, there are two effects on the amplitude in k space. One is the effect of neighboring atoms where the signal tends to increase in the entire k range with increasing coordination number, and the other is the effect of Debye-Waller factor, whose increment attenuates the amplitude at high k region.[21] A close inspection reveals that the HgI_2 intercalate shows smaller amplitude over the entire k range than the free $(Me_3S)_2HgI_4$ and its intercalate, which represents a smaller coordination number. It is also observed that the oscillation frequency is larger for the HgI_2 intercalate than for the other Hg-I species. This implies that the (Hg-I) bond length increases upon interlayer

TABLE II. The results of non-linear least square curve fitting for the first shell of Hg L_{III}-edge EXAFS spectra.

Compound	Bond distance(Å)	Coordination number	Debye-Waller factor (10^{-3} Å^2)
HgI_2	2.76_0	4[a]	7.27
HgI_2-Bi2212	2.64_7	2.06_6	6.86
$(Me_3S)_2HgI_4$	2.73_7	1[a]	5.12
	2.75_4	1[a]	5.12
	2.78_1	1[a]	5.12
	2.85_2	1[a]	5.12
$(Me_3S)_2HgI_4$-Bi2212	2.75_3	4.04_2	8.25

[a]The coordination numbers of references were fixed to the crystallographic value with a view to determining the amplitude reduction factor. The curve fitting analyses for these references were performed to the first coordination shell data.

complex-salt formation, which is also closely related to the changes in the coordination number. The best fitting results to the first coordination shell are compared to experimental spectra in Fig. 6(b), and the fitted structural parameters are summarized in Table II. The bond distances for the free $(Me_3S)_2HgI_4$ show only a small difference from previously reported crystallographic values,[41] which confirms the reliability of the present EXAFS analysis. Upon interlayer complex formation, the two-coordinated Hg in intracrystalline HgI_2 has changed to a four-coordinated HgI_4^{2-} unit and the average of the Hg-I bond length has been changed from 2.64 Å (HgI_2) to 2.75 Å (HgI_4^{2-}). As a result of this conversion from a molecular HgI_2 to HgI_4^{2-} anion, it is naturally expected that chemical interaction between host and guest should be modified, which in turn affects the physicochemical properties of the superconducting host lattice.

3. Bi L_{III}-edge XANES

The effect of HgI_2 or $(Me_3S)_2HgI_4$ intercalation on the electronic and local structures of the host lattice has been investigated by the comparative XANES studies at the Bi L_{III}-edge for the pristine Bi2212 and its intercalates. First, we put emphasis on the oxidation state and local environment of the Bi atom not only because the Bi-O plane is the very surface layer facing the guest species but also because the Bi-O and Cu-O bands are hybridized,[44,45] which gives rise to a change in superconducting property of the intercalated Bi2212 compounds. Taking a simple picture of crystal-field theory, the white line shapes of L_{III}-edge XANES spectra of heavy metals have been reported to represent the individual transitions to particular *d* orbitals that will occur at different energies in accordance with local symmetry around the absorbing atom.[46–48] Hence crystal-field splitting of unoccupied *d* orbitals can be probed by the L_{III}-edge XANES spectra. It is also a well-known fact that the crystal-field strength is dependent on both the metal-ligand bonding character and the oxidation state of the metal.

The Bi L_{III}-edge XANES splines and their second derivatives of the pristine Bi2212, HgI_2-Bi2212, and

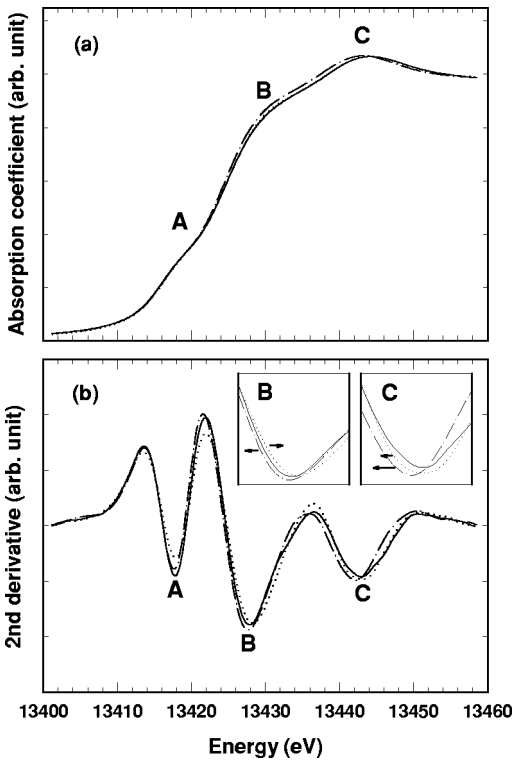

FIG. 7. (a) Bi L_{III}-edge XANES spectra for Bi2212 (solid lines), HgI_2-Bi2212 (dotted lines), and $(Me_3S)_2HgI_4$-Bi2212 (dash-dot lines) and (b) their second derivatives. The insets in (b) represent the enlarged second derivative spectra for peaks B and C.

$(Me_3S)_2HgI_4$-Bi2212 are shown in Figs. 7(a) and (b), respectively. A shoulder denoted by the pre-edge peak A, corresponding to the transition from $2p_{3/2}$ to $6s$ final state, is observed in all the pristine Bi2212 and intercalates. It is therefore concluded that some amounts of Bi(V) (less than 10%) are also present in the Bi-O layers of HgI_2 and $(Me_3S)_2HgI_4$ intercalates as well as in the pristine. The positions of pre-edge peak A for the pristine and its intercalates are not noticeably changed, but appreciable shifts in peaks B and C, corresponding to the transitions $2p_{3/2} \rightarrow 6d_{t_{2g}}$ and $2p_{3/2} \rightarrow 6d_{e_g}$ could be clearly observed. Peak B is slightly shifted toward the lower energy side ($\Delta E = -0.2$ eV) for the $(Me_3S)_2HgI_4$ intercalate compared to the pristine, whereas it is shifted toward higher energy side ($\Delta E = +0.4$ eV) for the HgI_2 intercalate. Such shifts toward opposite directions for two different types of intercalates indicate that the bismuth in Bi2212 is partially oxidized upon the HgI_2 intercalation, and slightly reduced upon the $(Me_3S)_2HgI_4$ intercalation. For the HgI_2 intercalate, an increase of the bismuth oxidation state gives rise to a higher energy of $2p_{3/2} \rightarrow 6d_{t_{2g}}$ transition, owing to an electronic charge transfer from the Bi-O layer to the intercalated HgI_2. For the organic-salt intercalate, on the contrary, a partial reduction of bismuth ion causes a slightly lowered final state level of $6d_{t_{2g}}$. Such an interpretation is based on the fact that a chemical shift to the t_{2g} state, which is less sensitive to the crystal field than the e_g one, is very linear against the change in oxidation state. Different from peak B, however, peak C shifts toward lower energy side for

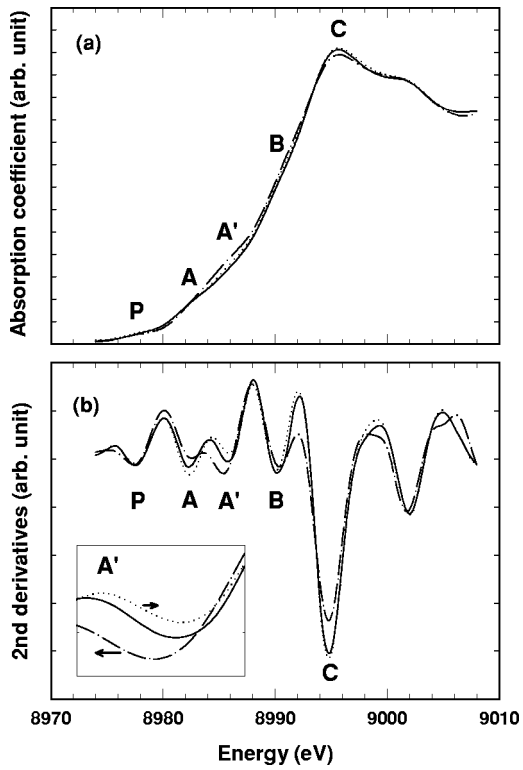

FIG. 8. (a) Cu *K*-edge XANES spectra for Bi2212 (solid line), HgI_2-Bi2212 (dotted line), and $(Me_3S)_2HgI_4$-Bi2212 (dash-dot line), and (b) their second derivatives. Peaks P, A, B, C, and A′ correspond to $1s\rightarrow 3d$, $1s\rightarrow 4p_\pi$ ($d^{10}\underline{L}$), $1s\rightarrow 4p_\pi$ (d^9), $1s\rightarrow 4p_\sigma$ (d^9), and $1s\rightarrow 4p_\sigma$ ($d^9\underline{L}$), respectively.

both types of intercalates, HgI_2 and $(Me_3S)_2HgI_4$ intercalates. Moreover, the position of peak C is systematically shifted toward the lower energy side from the pristine through HgI_2 intercalate ($\Delta E=-0.3$ eV) to the organic salt one ($\Delta E=-0.8$ eV), which reflects the change in crystal field around the bismuth atom upon intercalation. Especially, a weak interaction between bismuth and the guest is postulated to shift the e_g state level to a lower energy. Upon incorporating HgI_2 into the Bi_2O_2 double layers, oxygen of the longest Bi-O bond in the BiO_6 octahedron is replaced by iodine as schematically represented in Fig. 2. Since the electronegativity of iodine is quite smaller than that of oxygen, the crystal-field strength around the bismuth should decrease in the HgI_2 intercalate compared to the pristine. When the HgI_2 intercalate is transformed into the $(Me_3S)_2HgI_4$ one, the interaction between host and guest is further weakened due to the bulky anion of HgI_4^{2-}, which makes the crystal-field strength around the bismuth ion even smaller. These interpretations are well consistent with the empirical results from the Bi L_{III}-edge XANES spectra.

4. Cu K-edge XANES

Figures 8(a) and (b) represent the Cu *K*-edge XANES splines and second derivative spectra for the pristine Bi2212 and the intercalated samples, respectively. As shown in Fig. 8(a), the $(Me_3S)_2HgI_4$ intercalate exhibits characteristic peaks typically observed in the host, corresponding to the dipole allowed transitions from core $1s$ level to unoccupied $4p$ states, which are denoted as A, A′, B, and C, together with the pre-edge peak P corresponding to the $1s\rightarrow 3d$ transition. Although the pre-edge peak P is not a dipole allowed transition ($\Delta l\neq\pm 1$), it can be ascribed to a quadrupole-allowed transition and/or a hybridization of $4p$ and $3d$ states.[32,49] From the previous XAS studies on cuprate compounds with various oxidation states and local symmetries around copper ion,[32] it was known that the main-edge features A and B correspond to the transition from $1s$ core level to the out-of-plane $4p_\pi$ state, whereas the feature C is assigned as a transition to the in-plane $4p_\sigma$ one. Since the Coulombic energy between Cu $1s$ hole and $3d$ electron is much larger than the ligand to metal charge-transfer energy, the lower energy peak A could be assigned to the transition to the shakedown final state of $1s^13d^{10}4p_\pi^1\underline{L}$($\underline{L}$ represents a hole in the ligand) where an electron in oxygen $2p$ orbital is transferred to the copper $3d$ one.[32,50] In addition to these peaks (denoted as A, B, and C), the spectral feature corresponding to the transition from the $1s^23d^8$ to the $1s^13d^94p_\sigma^1\underline{L}$ state could be observed at around 8985.7 eV (denoted as $\overline{\text{A}}'$), which has been revealed as an indicator for the presence of the Cu^{+III} ion.[31,32]

Based on the above analyses, we have examined the effect of intercalation on the CuO_2 plane by comparing the Cu *K*-edge XANES spectra and their second derivatives among the pristine Bi2212, HgI_2-Bi2212, and $(Me_3S)_2HgI_4$-Bi2212, respectively. Peak A′ for the $(Me_3S)_2HgI_4$ intercalate shifts toward the lower energy side ($\Delta E=-0.4$ eV) with respect to that for the pristine, implying a partial reduction of the Cu^{+III} ion, while it is slightly shifted toward higher energy side ($\Delta E=+0.1$ eV) for the HgI_2 intercalate [Fig. 8(b)]. Former XAS studies for the HgX_2 (X=I, Br) intercalated Bi2212 revealed that electrons are transferred from the Bi2212 building block to the HgX_2 layer, leading to an increase of hole concentration in the CuO_2 plane.[6] Here, we suggest a mechanism that the electrons, transferred from the host to the intercalated HgI_2 layer, are transferred back to the cuprate block upon formation of $(Me_3S)_2HgI_4$ in between the Bi_2O_2 double layers. At this point, the reverse electron transfer in the $(Me_3S)_2HgI_4$ intercalate is attributed to a change in the molecular orbital derived from the electrostructural evolution from the linear HgI_2 to the tetrahedral HgI_4^{2-} unit. In this scheme, the frontier orbital interacting with the Bi-O plane is assumed to be the lowest unoccupied molecular orbital (LUMO) of HgI_2 and the highest occupied molecular orbital (HOMO) of HgI_4^{2-}, where the former acts as electron acceptor and the latter as electron donor.

The modification of hole density within the CuO_2 plane upon intercalation is quite well understood based on the theoretical background that the electronic structure of each sublayer in cuprate building block is not strictly Bi-O or Cu-O but an admixture due to the hybridization of Bi $6p$, Cu $3d$, and O $2p$ orbitals.[44,45] In fact, it has been already proposed that stoichiometric $Bi_2Sr_2CaCu_2O_8$ without excess oxygen becomes superconductive due to the hole doping in CuO_2 plane through internal redox equilibrium Bi(III)

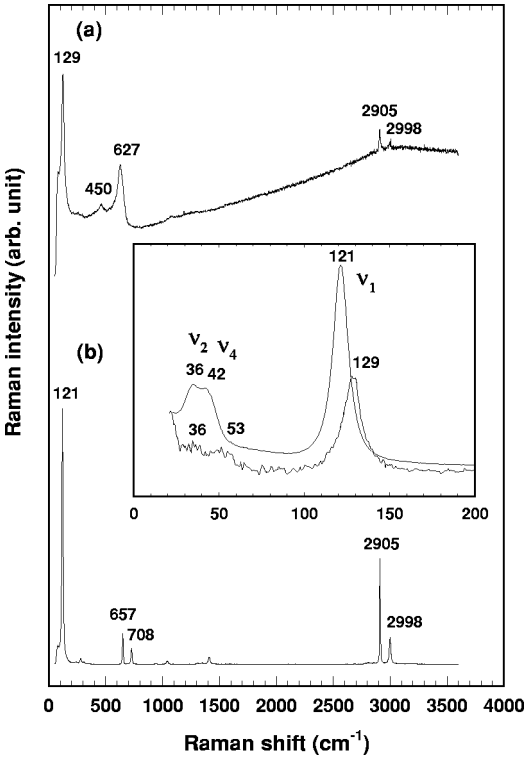

FIG. 9. Unpolarized micro-Raman spectra for (a) $(Me_3S)_2HgI_4$-Bi2212 and (b) free $(Me_3S)_2HgI_4$ compound, where the inset shows the Raman spectra corresponding to the HgI_4^{2-} vibration modes.

$+\mathrm{Cu(II)} \leftrightarrow \mathrm{Bi(III\text{-}}\varepsilon) + \mathrm{Cu(II}+\varepsilon)$.[44,45,51,52] In this regard, it is reasonable to consider that the hole density in CuO_2 plane is modified by the redox of Bi-O layer in close contact with the intercalated guests. The CuO_2 plane is believed to be partially oxidized upon HgI_2 intercalation, whereas it is slightly reduced upon $(Me_3S)_2HgI_4$ intercalation as was shown in XANES analyses at the Bi L_{III}- and Cu *K*-edges. However, the effect of intercalation on the CuO_2 layer is weaker than on the Bi-O one, because the former is separated from the latter by the Sr-O layer.

D. Raman analyses

A further evidence on the presence of $(Me_3S)_2HgI_4$ in between Bi_2O_2 layers could be provided by micro-Raman spectroscopy. Figure 9 represents the unpolarized micro-Raman spectra for $(Me_3S)_2HgI_4$-Bi2212 and free complex salt of $(Me_3S)_2HgI_4$. The Raman spectrum of complex-salt intercalate is compared with that of free $(Me_3S)_2HgI_4$ as a reference, where all the HgI_4^{2-} Raman bands of $(Me_3S)_2HgI_4$-Bi2212 show sharp features. As can be seen in Fig. 9, the main Raman bands of Me_3S^+ as well as HgI_4^{2-} are clearly observed in the complex-salt intercalate. The presence of $(Me_3S)_2HgI_4$ in between the Bi_2O_2 double layers is well demonstrated by the appearance of Raman bands at 2905 and 2998 cm^{-1} representing $-CH_3$ stretching vibrations of organic moiety and main band at 129 cm^{-1} due to the HgI_4^{2-} ion. As can be seen in the low-frequency range (inset of Fig. 9), not only the total symmetrical band ν_1 of the HgI_4^{2-} is seen but also the other vibrations ν_4 and ν_2 are detected at 53 and 36 cm^{-1}, respectively. This is proof that the symmetry of mercuric-iodide species still remains unchanged as tetrahedral. However, it is found that the ν_4 peak shifts from 42 to 53 cm^{-1} indicating a distortion of the tetrahedral unit in the present intercalate, especially with a change in the angles as this vibration is due mainly to a bending motion. In addition, the ν_1 vibration moves from 121 to 129 cm^{-1}, which is compatible with a compression of the unit by intercalation. These shifts of vibration modes reflect the change in the microenvironment around the HgI_4^{2-} ion in the $(Me_3S)_2HgI_4$ intercalate compared to the case of free $(Me_3S)_2HgI_4$.

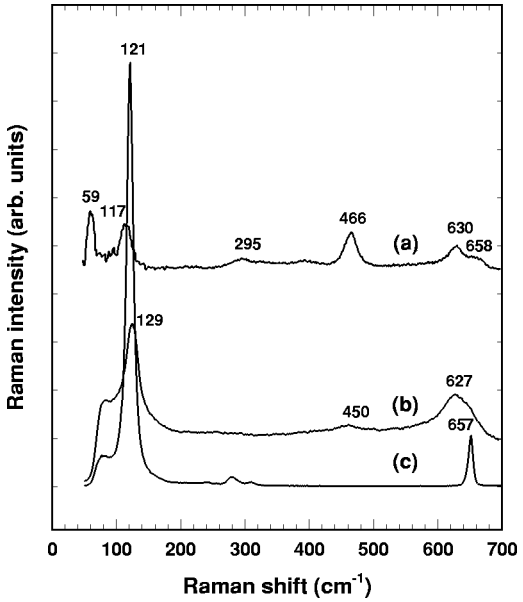

FIG. 10. Micro-Raman spectra for (a) Bi2212, (b) $(Me_3S)_2HgI_4$-Bi2212, and (c) free $(Me_3S)_2HgI_4$ in the frequency range of 50–700 cm^{-1}.

Figures 10(a)–(c) represent the Raman spectra for the pristine Bi2212, $(Me_3S)_2HgI_4$-intercalate, and free $(Me_3S)_2HgI_4$, respectively. The main Raman doublet around 659 and 630 cm^{-1} for the pristine Bi2212, corresponding to the two Bi-O bands, is collapsed into a single peak at 627 cm^{-1} in $(Me_3S)_2HgI_4$-Bi2212. It is well known that the doublet corresponds to the coupling of stretching motions in all bismuth-based superconductors representing close, staggered, and identical Bi-O layers along the *c* axis.[53–55] The disappearance of the higher frequency band at 659 cm^{-1} is therefore indicative of the motion decoupling of Bi-O bonds in $(Me_3S)_2HgI_4$-Bi2212. Such a spectral behavior indicates a change in space group from $I4mmm$ to $P4mmm$ due to a gliding of host lattice by $a/2$ with respect to the other upon intercalation. Furthermore, the phonon energy of the collapsed band in $(Me_3S)_2HgI_4$-Bi2212, 627 cm^{-1}, is slightly decreased when compared with the lower frequency band of the Raman doublet (659 and 630 cm^{-1}) for the pristine. A slight decrease in the Bi-O stretching frequency implies that the interaction between the intercalated $(Me_3S)_2HgI_4$ and adjacent Bi-O layer is very weak. It was also observed that the Bi-O stretching phonon shifts to lower

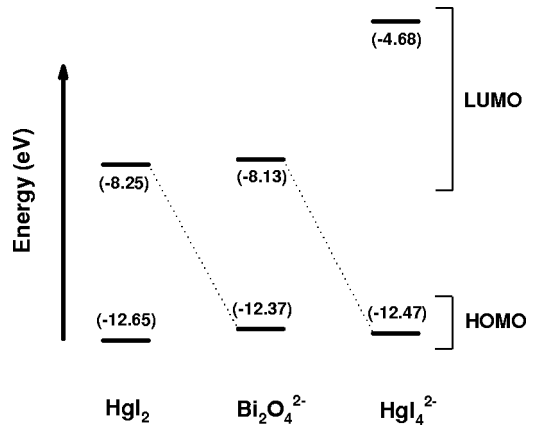

FIG. 11. HOMO's and LUMO's of $Bi_2O_4^{2-}$, HgI_2, and HgI_4^{2-}. The dotted lines represent the preferred interactions between the HOMO's and LUMO's.

energy side in the iodine intercalates compared to that of the pristine Bi2212, indicating a weak interaction between guest molecule and host Bi-O layer.[55] In the present intercalate, however, the guest $(Me_3S)_2HgI_4$ is composed of complex anion HgI_4^{2-} and organic cation Me_3S^+, which gives rise to a negligible bonding interaction between guest ions and the neighboring Bi-O layer.

E. Molecular-orbital calculations

In order to understand electronic interaction between host lattice and guest, molecular-orbital (MO) calculation was carried out for the HgI_2 intercalate and the $(Me_3S)_2HgI_4$ one. In the Bi-based cuprates, the Bi-O plane is the surface layer of cuprate building block, which is directly facing the intercalant layer. Therefore the chemical interaction between host and guest should be mainly affected by the relative electron donating or accepting ability, i.e., Lewis acidity and basicity, involving the orbitals of Bi-O layer and guest molecules. In the present Bi2212 interstratified with organic salt, while the organic cation Me_3S^+ is intercalated in the form of $(Me_3S)_2HgI_4$, its contribution to the Lewis acid-base interaction is supposed to be negligible compared to the highly polarizable HgI_4^{2-} anion. In this context, the molecular orbitals (MO's) of the HgI_2 molecule and the HgI_4^{2-} anion were calculated on the basis of geometric parameters such as coordination number and bond length (Hg-I), which were derived from the Hg L_{III}-edge EXAFS analyses of the corresponding intercalates, and compared to the energy level of the Bi-O layer, which was approximated as $Bi_2O_4^{2-}$ cluster. In this work, the MO calculations were performed by the extended Hückel tight-binding band calculation method.

In Fig. 11, the relative energy levels in the $Bi_2O_4^{2-}$ cluster MO are represented, together with those in HgI_2 and HgI_4^{2-} MO's. The highest occupied molecular orbital (HOMO) and lowest unoccupied molecular orbital (LUMO) of the $Bi_2O_4^{2-}$ cluster are determined to be -12.37 and -8.13 eV, respectively, whereas those of HgI_2 molecule are -12.65 and -8.25 eV. For the pair of $Bi_2O_4^{2-}$ and HgI_2, the LUMO of each species is higher than the HOMO of the counterpart by more than 4 eV. The $Bi_2O_4^{2-}$(HOMO)-HgI_2(LUMO) perturbation will be more favorable than the case of $Bi_2O_4^{2-}$(LUMO)-HgI_2(HOMO) one, because the energy difference for the former (4.12 eV) is smaller than for the latter (4.52 eV). According to this reasoning, the HOMO of $Bi_2O_4^{2-}$ behaves as a donor orbital and the LUMO of HgI_2 as an acceptor orbital. The electrons therefore could be preferably transferred from the $Bi_2O_4^{2-}$ cluster to the HgI_2 layer upon intercalation and, as a consequence, the Bi-O layer is slightly oxidized.[6]

On the other hand, the calculated MO of HgI_4^{2-} anion is markedly different from that of HgI_2 molecule (Fig. 11), due to the change in molecular structure and coordination number from linear HgI_2 to tetrahedral HgI_4^{2-}. The LUMO level is raised from -8.25 eV for the HgI_2 to -4.68 eV for the HgI_4^{2-}, whereas the HOMO level is only slightly changed from -12.65 to -12.47 eV. Hence the HgI_4^{2-}(HOMO)-$Bi_2O_4^{2-}$(LUMO) interaction should be more favored than the HgI_4^{2-}(LUMO)-$Bi_2O_4^{2-}$(HOMO) one, where the HOMO of HgI_4^{2-} acts as the donor orbital and the LUMO of $Bi_2O_4^{2-}$ (LUMO) as the acceptor orbital leading to a partial electron transfer from HgI_4^{2-} anion to $Bi_2O_4^{2-}$ cluster, i.e., to the Bi-O layer. Based on the concept of HOMO-LUMO interaction as mentioned above, it is found that the Bi-O layer can function as either a Lewis base for the HgI_2 molecule or a Lewis acid for the HgI_4^{2-} anion. Such theoretical results have been actually confirmed by the Bi L_{III}- and I L_I-edge XANES analyses for the HgI_2 intercalate and the $(Me_3S)_2HgI_4$-one. Thus the perturbational MO approach provides a tentative but simple solution to the problems of electronic charge transfer between host and guest, which in turn gives a qualitative explanation for the T_c variations upon intercalation.

IV. CONCLUSION

We have successfully developed a heterostructured nanohybrid between the Bi-based high-T_c superconductor (Bi2212) and insulating organic salt through an interesting stepwise intercalation route. The present organic-salt intercalation compound is different in its *S-I-S* multilayered structure and is an ideal model compound for studying high-T_c superconductivity, since the charge-carrying cuprate sheets are separated by the insulating ionic layer with atomically precise interface. From the physicochemical characterizations of the present intercalate, it is revealed that the anisotropy and electronic structures of layered cuprate can be controlled by intercalation reaction, because the interstratification of guest into the Bi2212 lattice modifies not only the layer separation between cuprate block but also the charge-carrier density of the superconducting layer. Both the partial oxidation and reduction of the cuprate block could be feasible depending on the nature of the intercalant. Compared to the pristine Bi2212, the onset T_c value increases slightly in spite of remarkable basal increment ($\Delta d = 12.6$ Å) upon $(Me_3S)_2HgI_4$ intercalation, whereas T_c is depressed by ~ 10 K upon mercuric iodide intercalation ($\Delta d = 7.2$ Å). The main cause of T_c variation in these intercalates is attributed to the modification of hole density in the

CuO_2 plane not only due to the hybridization between the Bi-O and Cu-O bands but also due to the electronic charge transfer between Bi-O layer and the guests, those which are empirically confirmed by Bi L_{III}- and Cu *K*-edge XANES analyses for the HgI_2- and $(Me_3S)_2HgI_4$-intercalated Bi2212, and theoretically verified by MO calculations for the host and the guest species. The Raman and EXAFS studies on the present nanohybrid reveal that the intercalated organic moiety is stabilized as a complex salt of $(Me_3S)_2HgI_4$. In addition, the synthetic strategy of interlayer complexation adopted in this work could open a different way of preparing organic-inorganic hybrid materials with a molecular-level layer-by-layer structural feature, having advantageous properties both from crystalline inorganic solids and from organic components. In the present study, it is demonstrated that the organic-salt compound can also be used to tailor the electronic properties of the cuprate layer through host-guest interaction and to modulate the electronic coupling between superconducting layers by modifying the interlayer separation.

ACKNOWLEDGMENTS

Financial support from the Ministry of Science and Technology through the National Research Laboratory program is gratefully acknowledged. One of the authors (S.J.K.) thanks Dr. N. H. Hur, Korea Research Institute of Standards and Science, for the SQUID measurements. We thank the Photon Factory, National Laboratory for High Energy Physics and are grateful to Professor M. Nomura for his help in x-ray-absorption experiments. Experimental help from W. H. Ahn in materials preparation is also acknowledged.

*Electronic address: sjk0515@unitel.co.kr

[1] X. D. Xiang, S. Mckernan, W. A. Vareka, A. Zettl, J. L. Corkill, T. W. Barbee III, and M. L. Cohen, Nature (London) **348**, 145 (1990).

[2] X. D. Xiang, W. A. Vareka, A. Zettl, J. L. Corkill, T. W. Barbee III, M. L. Cohen, N. Kijima, and R. Gronsky, Science **254**, 1487 (1991).

[3] X. D. Xiang, A. Zettl, W. A. Vareka, J. L. Corkill, T. W. Barbee III, and M. L. Cohen, Phys. Rev. B **43**, 11 496 (1991).

[4] J. H. Choy, S. J. Kwon, and G. S. Park, Science **280**, 1589 (1998).

[5] J. H. Choy, N. G. Park, S. J. Hwang, D. H. Kim, and N. H. Hur, J. Am. Chem. Soc. **116**, 11 564 (1994).

[6] J. H. Choy, S. J. Hwang, and N. G. Park, J. Am. Chem. Soc. **119**, 1624 (1997).

[7] J. H. Choy, N. G. Park, Y. I. Kim, S. H. Hwang, J. S. Lee, and H. I. Yoo, J. Phys. Chem. **99**, 7845 (1995).

[8] J. H. Choy, N. G. Park, S. J. Hwang, and Z. G. Khim, J. Phys. Chem. **100**, 3783 (1996).

[9] J. H. Choy, S. J. Hwang, and D.-K. Kim, Phys. Rev. B **55**, 5674 (1997).

[10] J. H. Choy, S. J. Kwon, S. J. Hwang, Y. I. Kim, and W. Lee, J. Mater. Chem. **9**, 129 (1999).

[11] J. H. Choy, Y. I. Kim, S. J. Hwang, and I. S. Yang, J. Solid State Chem. **147**, 328 (1999).

[12] J. M. Wheatly, T. C. Hsu, and P. W. Anderson, Nature (London) **333**, 121 (1988).

[13] G. Liang, A. Sahiner, M. Croft, W. Xu, X. D. Xiang, D. Badresingh, W. Li, J. Chen, J. Peng, A. Zettl, and F. Lu, Phys. Rev. B **47**, 1029 (1993).

[14] Y. J. Uemura *et al.*, Phys. Rev. Lett. **62**, 2317 (1989).

[15] J. Ihm and B. D. Yu, Phys. Rev. B **39**, 4760 (1989).

[16] Q. Li *et al.*, Phys. Rev. Lett. **64**, 3086 (1990); D. R. Harshman and A. P. Mills, Jr., Phys. Rev. B **45**, 10 684 (1992).

[17] R. Arnek and D. Poceva, Acta Chem. Scand., Ser. A **30**, 59 (1976).

[18] H. Maeda, T. Tanaka, M. Fukutomi, and T. Asano, Jpn. J. Appl. Phys., Part 2 **27**, L209 (1987).

[19] F. W. Lytle, G. van der Laan, R. B. Greegor, E. M. Larson, C. E. Violet, and J. Wong, Phys. Rev. B **41**, 8955 (1990).

[20] E. A. Stern and K. Kim, Phys. Rev. B **23**, 3781 (1981).

[21] B. K. Teo, *EXAFS: Basic Principles and Data Analysis* (Springer-Verlag, Berlin, 1986).

[22] J. J. Rehr, Jpn. J. Appl. Phys., Part 1 **32**, 8 (1993); J. J. Rehr, R. C. Albers, and S. I. Zabinsky, Phys. Rev. Lett. **69**, 3397 (1992).

[23] S. D. Obertelli, J. R. Cooper, and J. L. Tallon, Phys. Rev. B **46**, 14 928 (1992).

[24] M. R. Presland, J. L. Tallon, R. G. Buckley, R. S. Liu, and N. E. Flower, Physica C **176**, 95 (1991).

[25] W. A. Groen, D. M. de Leeuw, and L. F. Feiner, Physica C **165**, 55 (1990); M. Nagoshi, T. Suzuki, Y. Fukuda, K. Terashima, Y. Nakanishi, M. Ogita, A. Tokiwa, Y. Syono, and M. Tachiki, Phys. Rev. B **43**, 10 445 (1991).

[26] J. R. Clem and M. W. Coffey, Phys. Rev. B **42**, 6209 (1990).

[27] M. K. Bae, M. S. Kim, S. I. Lee, N. G. Park, Seong-Ju Hwang, D. H. Kim, and J. H. Choy, Phys. Rev. B **53**, 12 416 (1996).

[28] P. H. Kes, J. Aarts, V. M. Vinokur, and C. J. VanderBeek, Phys. Rev. Lett. **64**, 1063 (1990).

[29] D. N. Basov, T. Timusk, B. Dabrowski, and J. D. Jorgensen, Phys. Rev. B **50**, 3511 (1994).

[30] Y. J. Uemura, Physica C **282-287**, 194 (1997).

[31] J. H. Choy, D. K. Kim, S. H. Hwang, and J. C. Park, J. Am. Chem. Soc. **117**, 7556 (1995).

[32] J. H. Choy, D. K. Kim, S. H. Hwang, and G. Demazeau, Phys. Rev. B **50**, 16 631 (1994).

[33] J. H. Choy, J. B. Yoon, D. K. Kim, and S. H. Hwang, Inorg. Chem. **34**, 6524 (1995).

[34] S. J. Hwang, N. G. Park, D. H. Kim, and J. H. Choy, J. Solid State Chem. **138**, 66 (1998).

[35] J. H. Choy, Y. I. Kim, and S. J. Hwang, J. Phys. Chem. **102**, 9191 (1998).

[36] D. E. Turner and B. N. Harmon, Phys. Rev. B **40**, 10 516 (1989).

[37] N. G. Park, S. W. Cho, S. J. Kim, and J. H. Choy, Chem. Mater. **8**, 324 (1996).

[38] R. Åkesson, I. Persson, M. Sandström, and U. Wahlgren, Inorg. Chem. **33**, 3715 (1994).

[39] T. Yamamura, T. Watanabe, A. Kikuchi, M. Ushiyama, T. Kobayashi, and H. Hirota, J. Phys. Chem. **99**, 5525 (1995).

[40] A. F. Wells, *Structural Inorganic Chemistry* (Clarendon Press, Oxford, 1984), p. 1162.

[41] R. H. Fenn, Acta Crystallogr. **20**, 24 (1966).

[42] M. Sandström, I. Persson, and P. Persson, Acta Chem. Scand. **44**, 653 (1990).
[43] N. F. Mott, *The Theory of Atomic Collisions* (Clarendon Press, Oxford, 1965).
[44] F. Herman, R. V. Kasowski, and W. Y. Hsu, Phys. Rev. B **38**, 204 (1988); R. Retoux, F. Studer, C. Michel, B. Raveau, A. Fontaine, and E. Dartyge, *ibid.* **41**, 193 (1990); A. Q. Pham, F. Studer, N. Merrien, A. Maignan, C. Michel, and B. Raveau, *ibid.* **48**, 1249 (1993).
[45] W. E. Pickett, Rev. Mod. Phys. **61**, 433 (1989).
[46] G. van der Laan, B. T. Thole, G. A. Sawatzky, and M. Verdaguer, Phys. Rev. B **37**, 6587 (1988).
[47] J. Evans, J. Frederick, and W. Mosselmans, J. Phys. Chem. **95**, 9673 (1991).
[48] S. R. Bare, G. E. Mitchell, J. J. Maj, G. E. Vrieland, and J. L. Gland, J. Phys. Chem. **97**, 6048 (1993).
[49] E. Hahn, R. A. Scott, K. O. Hodgson, S. Doniach, S. R. Desjardins, and E. I. Solomon, Chem. Phys. Lett. **88**, 595 (1982).
[50] N. Kosugi, H. Kondoh, H. Tajima, and H. Kuroda, Chem. Phys. **135**, 149 (1989).
[51] M. S. Hybertsen and L. F. Mattheiss, Phys. Rev. Lett. **60**, 1661 (1988).
[52] A. Q. Pham, A. Maignan, M. Hervieu, C. Michel, J. Provost, and B. Raveau, Physica C **191**, 77 (1992).
[53] P. V. Huong, Physica C **180**, 128 (1991).
[54] P. V. Huong, A. L. Verma, R. Cavagnat, H. Kitahama, T. Kawai, M. Lahaye, and E. Marquestaut, J. Alloys Compd. **195**, 133 (1993).
[55] P. V. Huong and A. L. Verma, Phys. Rev. B **48**, 9869 (1993).